Heliyon 6 (2020) e04875

Contents lists available at ScienceDirect

Heliyon

journal homepage: www.cell.com/heliyon

Research article

Magneto-hydro dynamic squeezed flow of Williamson fluid transiting a sensor surface

Azad Hussain [a,*], Rabia Zetoon [a], Shoaib Ali [a], S. Nadeem [b]

[a] Department of Mathematics, University of Gujrat, Gujrat 50700, Pakistan
[b] Department of Mathematics, Quaid-i-Azam University, Islamabad 44000, Pakistan

ARTICLE INFO

Keywords:
Applied mathematics
Mechanical engineering
Thermodynamics
Sensor surface
Squeezed flow
MHD Flow
Variable thermal conductivity

ABSTRACT

The present article reports the combined effects of radiation and heat origination on the electro-kinetically induced hydromagnetic squeezed flow of a pseudoplastic fluid. The fluid is passing over a microcantilever sensor surface positioned in the superficial free stream. Microcantiliver sensor can detect the flow rate and the variance in the temperature of the fluid. The thermal conductivity and fluid viscosity are assumed as a function of temperature. Boundary layer approximations are considered to construct a pseudoplastic fluid flow model. The governing system is then resolved into a non-dimensional form with the assistance of an appropriate set of control parameters. The solution to these non-dimensional equations has calculated with the assistance of familiar numerical techniques i.e. Shooting technique. The results specify that flow of fluid, temperature, and velocity profiles are remarkably influenced by the radiation parameter, fluid parameter, heat generation parameter, thermal relaxation parameter, magnetic parameter, and the squeezing number. A comprehensive graphical and tabular study is constructed to check the convergence of the obtained results. One can detect that the temperature curve is changing slightly for the Christov-Cattaneo heat transfer model as compared to classical Fourier's law of heat transfer. Further, the physical quantities, i.e. free stream velocity, variable viscosity, thermal conductivity, Weissenberg number, and Prandtl number have strong impacts on the boundary layer flow equations. It is perceived that the fluid velocity profile rises for the growing value of the magnetic parameter, but reduces for squashed flow index b. Also, a positive variation is found in the temperature profile for rising values of β and Q.

1. Introduction

The exploration of boundary layer squeezing liquid flow and heat transference passing through a sensor surface is a most fascinating research topic due to the fact of its broad range utilization in engineering and industry. The most common engineering and scientific applications are manufacturing of polymer, food processing, lubrication system, cooling towers, hydro machines, marine engineering, distillation columns, and so on. M. Usman et al. [1] deliberated the heat and flow characteristics of Cu-nano particles immersed in the water among the two squeezing permeable disks. M. Atlas et al. [2] inspected the sway of thermic radiation on the change of nanoparticle quantity among a squashing channel. M. Khan et al. [3] worked on the transfer of heat during the Williamson nanofluid flow under Lorentz force passing through a stretching surface. The thermic characteristics of nanofluid among two plates have inspected by Ganji and Sheikholeslami [4].

The recent revolution in technology has required advancement in the sensor surfaces. Predominantly, micro-cantilever sensors are distinguished from the others due to their biological, physical, and chemical sensing. They also have a broad range of utilizations in the area of medicine, precisely for the detecting of diseases, blood glucose observing, tracing of chemical, exposure of point mutations, and biomedical warfare agents. These types of sensors have numerous benefits over the conventional methods in terms of minimum cost, simple methods, high sensitivity, non-hazardous techniques, and rapid response. Microcantilever supported sensors are the finest MEMS gadgets that are capable of ensuring a brightening future for the progress of new physical, biological, and chemical sensors. These are the most updated analyst detection systems in the class of most modern systems currently employed. They have significant potential for the exposure of different analytes in a vacuum, gaseous and liquid mediums. They can sense the flow rate of fluid and the variance in temperature to the small range 5–10 K and able to detect the photothermal measurement. Bimetallic

* Corresponding author.
E-mail address: azad.hussain@uog.edu.pk (A. Hussain).

https://doi.org/10.1016/j.heliyon.2020.e04875
Received 28 August 2018; Received in revised form 24 January 2019; Accepted 4 September 2020

microcantilevers can calculate photothermal spectroscopy with an accuracy of 150 fJ. They are capable of detecting heat transfer with sensitivity in atto joule. Furthermore, in the recent few years, the technology has grown for the usage of nano-cantilevers and fabrication and the sensing applications, thus producing nano-electromechanical systems. This advancement has enhanced the sensitivity to the maximum extent that researchers are now able to visualize the calculation of molecules. With the ability of high ultra-sensitive detection, this technology embraces the remarkable potential for the coming generation extremely sensitive sensors. Haq et al. [5] stated about the squeezed transference behavior of nanofluid over a sensor-based surface subjected to a transverse magnetic field. K. Ganesh Kumar et al. [6] explored the boundary layer squeezing movement of a conducting liquid under the magnetic influence transiting a sensor material. Khan et al. [7] probed numerically the heat transference in the squashed flow of Carreau type fluid traversing a sensor material with variable thermic conductivity. Rashidi et al. [8] expressed the influence of magnetic, suction, and injection effects on the squashed flow across sensor the surface.

MHD flow has a significant role in several areas like geophysics, engineering, astrophysics, and industrial processes comprising flow meters, nuclear reactors, driven processes, and MHD generators, etc. Many applications of electromagnetic fields have strong influences on the flow behavior of fluids like electrolytes, molten metals, plasma, and various others. Many fluids are not always strong conductors of electricity, so their conductivity can be improved by introducing electric field externally. Imad Khan et al. [9] deliberated numerically the MHD stream of Carreau type fluid through a stretching cylinder with heterogeneous and homogenous reactions. S. Bilal [10] analyzed the hydromagnetic transference of Williamson type fluid owing to the bidirectional stretching surface with chemical substances. Malik et al. [11] inspected the influences of variable thermic conductivity and generation/absorption of heat transmission on MHD 3-D transport of Williamson liquid owing to bidirectional nonlinear stretching surface.

The transmission of mass and heat occur commonly in several manufacturing procedures, technological and industrial processes like marine engineering, pharmaceutical, glass products, sheeting substances, crystal growing, nuclear reactor, and petroleum industries, etc. Due to the influence of heat transfer in many applications, many researchers [5, 12, 13, 14, 15, 16, 17] have discovered the diverse technological and physical features about the problems involving the shrinking and stretching of boundaries, heat generation effects, magneto hydrodynamics, transmission of wall mass, radiation effects, diffusion-thermo influences, and thermal-diffusion influences, etc. Most of the investigations [5,12, 13, 14, 15, 16, 17] executed until now frequently integrate conventional mass and heat transfer theories but by altering the relaxation times parameter for velocity profiles, the temperature profile experience eventual effects, thus the thermal heat transfer must be considered. Cattaneo [18] scrutinized the conduction of heat using the Fourier's law and analyzed that the modification of Fourier's law can be done by presenting thermal relaxation time in Fourier's law. A further modification was made by Christov [19] for achieving the formulation of material invariant by including the upper convective derivative of Oldroyd. Malik et al. [20] deliberated the hydromagnetic transference of blood type fluid with the CCHF model taking temperature varying viscosity. T. Salahuddin et al. [21] reviewed the sway of the magnetic field on Williamson type fluid transference with the CCHF model traversing through a stretching sheet. T. Hayat et al. [22] comprehensively calculated the transport of fluid over a thicker surface with the compliance of the CCHF model. T. Hayat et al. [23] characterized the significance of the CCHF model on the stagnation transport of fluid. Muhammad Ijaz Khan et al. [24] calculated a comparative analysis of blood type fluid in compliance with heterogeneous-homogeneous reactions. Many other efforts regarding the flow analysis of fluids using numerical techniques are accessible in studies [25, 26, 27, 28, 29, 30]. Zahir Shah et al. [31] inspected the Darcy-Forchheimer streaming of micropolar Ferrofluid by applying the CCHF model. They also made useful studies [32, 33, 34] for investigating the dynamics of nano-fluids with the assistance of CCHF model.

The determination of this effort is to scrutinize the heat transfer and momentum characteristics to the squeezed flow of pseudo-plastic fluid traversing through a sensor-based surface in the presence of magnetic consequences acting transversely to the flow. The flow is driven by the mutual effects of thermal radiations and heat generation. Moreover, an advanced heat flux model is used to develop the energy equation for the analysis of heat conduction.

2. Mathematical modeling of the problem

We analyze the incompressible squeezed movement of electrically conducting Williamson fluid through a sensor surface closed in a squeezing channel. Electro-kinetically induced MHD flow is driven by heat generation and radiation effects. Fluids with greater conductivity σ (e.g. molten metals and semiconductor melts) ($\sigma \sim 106S/m$) can greatly be influenced by ~1 T external magnetic field strength. This is considered while controlling the classical magneto-hydrodynamic flow. But in the case of lightly conducting fluids (e.g. the water of sea having $\sigma \sim 10$ S/m) the superficial magnetic field is unable to induce the current. This problem is tackled by introducing an external electric field.

We presume that the sensor surface is located inside squeezed duct in such a way that height h(t) of the sensor plate is bigger than the width of the boundary layer.

We have transformed the energy, continuity, and momentum equations in the following form with the assistance of boundary layer estimations [16].

$$\frac{\partial v}{\partial y}+\frac{\partial u}{\partial x}=0, \tag{1}$$

$$\frac{\partial u}{\partial x}u+\frac{\partial u}{\partial t}+\frac{\partial u}{\partial y}v=-\frac{1}{\rho}\frac{\partial p}{\partial x})+\frac{\mu_0}{\rho}\frac{\partial^2 u}{\partial y^2}+\frac{1}{\rho}\frac{\partial \mu_0}{\partial y}\frac{\partial u}{\partial y}+\frac{1}{\sqrt{2}\rho}\Gamma\frac{\partial \mu_0}{\partial y})(\frac{\partial u}{\partial y})^2 +\sqrt{2}\Gamma\frac{\mu_0}{\rho}(\frac{\partial u}{\partial y})(\frac{\partial^2 u}{\partial y^2})-\frac{\sigma_m B_m^2 u}{\rho}, \tag{2}$$

Velocity in free stream

$$U\frac{\partial U}{\partial x}+\frac{\partial U}{\partial t}=-\frac{1}{\rho}(\frac{\partial p}{\partial x})-\frac{\sigma_m B_m^2 U}{\rho}, \tag{3}$$

From Eqs. (2) and (3) after terminating the pressure gradient the momentum equation takes the form

$$v\frac{\partial u}{\partial y}+u\frac{\partial u}{\partial x}+\frac{\partial u}{\partial t}=\frac{\partial U}{\partial t}+\frac{\sigma_m B_m^2(U-u)}{\rho}+U\frac{\partial U}{\partial x}+\frac{\mu_0}{\rho}\frac{\partial^2 u}{\partial y^2}+\frac{1}{\rho}\frac{\partial u}{\partial y}\frac{\partial \mu_0}{\partial y} +\frac{1}{\sqrt{2}\rho}\Gamma(\frac{\partial \mu_0}{\partial y})(\frac{\partial u}{\partial y})^2+\sqrt{2}\Gamma\frac{\mu_0}{\rho}(\frac{\partial u}{\partial y})(\frac{\partial^2 u}{\partial y^2}). \tag{4}$$

In literature, other models such as Vogel's and Reynolds' models have also been applied, but it is investigated that they provide significant results for a specific temperature range [35]. So, we have used the more accurate viscosity model as compared to Reynolds and Vogel's models which are capable of comprising a large temperature range. It is more suitable to express the viscosity coefficient μ as a reciprocal function of temperature [36],

$$\frac{1}{\mu}=\frac{1}{\mu^*}[1+\gamma(T-T_\infty)] \quad \text{i.e.} \quad \frac{1}{\mu^*}=c(T-T_r), \qquad c=\frac{\gamma}{\mu^*} \quad \text{and} \quad T_r=T_\infty-\frac{1}{\gamma}. \tag{5}$$

Both the constant c and T_r depend upon the thermal characteristic of the fluid, i.e., γ. Commonly $c>0$ epitomizes for fluids, while $c<0$ for

gases. Here, μ^* characterizes the constant viscosity of fluid at superficially free stream. Using Eq. (5) in Eq. (3) we obtain

$$\frac{\partial u}{\partial t}+u\frac{\partial u}{\partial x}+v\frac{\partial u}{\partial y}=\frac{\partial U}{\partial t}+U\frac{\partial U}{\partial x}+\left(\frac{1}{\rho c(T-T_r)}\right)\left(\frac{\partial^2 u}{\partial y^2}\right)+\frac{1}{\rho}\frac{\partial}{\partial y}\left(\frac{1}{c(T-T_r)}\right)\frac{\partial u}{\partial y}$$
$$+\frac{\sigma_m B_m^2(U-u)}{\rho}+\sqrt{2}\Gamma\frac{1}{\rho c(T-T_r)}\left(\frac{\partial u}{\partial y}\right)\left(\frac{\partial^2 u}{\partial y^2}\right)$$
$$+\frac{1}{\sqrt{2}\rho}\Gamma\frac{\partial}{\partial y}\left(\frac{1}{c(T-T_r)}\right)\left(\frac{\partial u}{\partial y}\right)^2 \tag{6}$$

corresponding boundary conditions are as

$$u(x,\,0,\,t)=0,\quad v(x,\,0,\,t)=v_0(t),\quad u(x,\infty,\,t)=U(x,\,t). \tag{7}$$

When the sensor surface is penetrable then velocity at the sensor surface is considered as reference velocity $v_0(t)$.

To scrutinize heat transference characteristics, non-Fourier heat transfer model is applied for evaluating heat transference during fluid flow. For incompressible fluid, the model changes into

$$\mathbf{q}+\delta_c\left[\mathbf{V}.\nabla\mathbf{q}+\frac{\partial\mathbf{q}}{\partial\mathbf{t}}-\mathbf{q}.\nabla\mathbf{V}\right]=-K\nabla T. \tag{8}$$

Here δ_c,$\mathbf{V}$ and K represent the thermal relaxation time, fluid velocity and the thermal conductivity.

For the present flow phenomenon, the above equation can be written as

$$v\frac{\partial T}{\partial y}+u\frac{\partial T}{\partial x}+\frac{\partial T}{\partial t}+\lambda_c\Omega_c=\frac{\partial}{\partial y}(\alpha\frac{\partial T}{\partial y})+\frac{Q_0}{\rho C_p}(T-T_\infty)-\frac{1}{\rho C_p}.\frac{\partial q_r}{\partial y}, \tag{9}$$

$\alpha(T)$ is the variable thermic conductivity defined as $\alpha(T)=\alpha_\infty(1+\varepsilon\,\Theta)$, t signifies time, T indicates temperature, $\alpha=\frac{k}{\rho C_p}$ symbolizes thermal diffusivity, and C_p illustrates specific heat, q_r characterizes the radiative flux q.

The value of Ω_c specified as

$$\Omega_c=\frac{\partial^2 T}{\partial t^2}+u\frac{\partial T}{\partial x}\frac{\partial u}{\partial x}+v\frac{\partial T}{\partial y}\frac{\partial v}{\partial y}+\frac{\partial u}{\partial t}\frac{\partial T}{\partial x}+v^2\frac{\partial^2 T}{\partial y^2}+2u\frac{\partial^2 T}{\partial x\partial t}+2uv\frac{\partial^2 T}{\partial x\partial y}$$
$$+u\frac{\partial T}{\partial y}\frac{\partial v}{\partial x}+\frac{\partial T}{\partial y}\frac{\partial v}{\partial t}+v\frac{\partial T}{\partial x}\frac{\partial u}{\partial y}+2v\frac{\partial^2 T}{\partial y\partial t}+u^2\frac{\partial^2 T}{\partial x^2}. \tag{10}$$

The boundary conditions associated with the system are stated as

$$T(x,\infty,\,t)=T_\infty,\quad -k\frac{\partial T(x,\,0,\,t)}{\partial y}=q(x). \tag{11}$$

Here, $q(x)$ and T_∞ signify wall heat transfer and ambient temperature, respectively.

Roseland approximation

$$q_r=\frac{-4}{3}.\frac{\sigma^*}{KR^*}.\frac{\partial T^4}{\partial y}. \tag{12}$$

For the smaller variation in temperature during flow, we can easily use the Taylor series to expand T_4 about T_∞ and by neglecting the unnecessary terms we get

$$T^4\cong 4T_\infty^3T-3T_\infty^4. \tag{13}$$

The transformation procedure

$$U=ax,\ u=axf'(\xi),\quad \xi=y\sqrt{\frac{a}{\upsilon}},\quad v=-f(\xi)\sqrt{a\upsilon},$$
$$\Theta(\xi)=\frac{T-T_\infty}{q_o x\sqrt{\frac{\upsilon}{a}}},\quad \psi=x\sqrt{a\upsilon}f(\xi),\quad a=\frac{1}{(s+bt)} \tag{14}$$

where $v_0(t)=v\sqrt{a}$, $q(x)=q_0x$, s is an arbitrary constant, b represents squeezed flow index, k is thermal conductivity, q_0 indicates heat flux and a depicts squeezing ability parameter. Using Eqs. (12) and (13) in Eq. (9) and by applying transformations to Eqs. (6) and (9) we get

$$(1+\sqrt{2}W_e^2f'')f'''-\frac{\Theta'}{\Theta-\Theta_r}f''-\frac{1}{\sqrt{2}}W_e^2\frac{\Theta'}{\Theta-\Theta_r}(f'')^2$$
$$+\frac{\Theta-\Theta_r}{\Theta_r}[(f')^2-\frac{b\xi}{2}f''-1+b(1-f')-ff''+M(f'-1)-ff'']=0 \tag{15}$$

$$(1+R+\varepsilon\Theta-\frac{\beta b^2\mathrm{Pr}\xi^2}{4}-\beta\mathrm{Pr}f^2-\beta b\mathrm{Pr}\xi f)\Theta''+\mathrm{Pr}(f+\frac{b\xi}{2}-\frac{\beta b^2\xi}{4}+3\beta ff'$$
$$+\frac{\beta b\xi f'}{2}-\frac{\beta bf}{2})\Theta'+\mathrm{Pr}(f'-\frac{b}{2}+\frac{\beta b^2}{4}-\beta f^2+\frac{\beta b\xi f''}{2}+\beta bf'-\beta bf+\beta ff''+Q)\Theta=0, \tag{16}$$

and related transformed boundary conditions are

$$f(0)=-f_0,\quad f'(\infty)\to 1,\quad f'(0)=0,$$
$$\Theta'(0)=-1,\quad \Theta(\infty)\to 0, \tag{17}$$

here, $f_0=\sqrt{\upsilon}$ is permeable velocity, $M=\frac{\sigma_m B_m^2}{\rho a}$ is the Hartmann number, $\mathrm{Pr}=\frac{\upsilon}{\alpha_\infty}$ represents Prandtl number, $R=\frac{16\sigma^*\Theta_\infty^3}{3\alpha_\infty K^*}$ shows radiation parameter, $Q=\frac{Q_0}{a\rho C_p}$ indicates heat generation parameter, $\Theta_r=\frac{1}{\gamma(T_w-T_\infty)}$ a parameter representing the fluid viscosity, $\beta=a\,\lambda$ is the dimensionless heat relaxation parameter, ε is a small quantity and $W_e=\frac{\Gamma a^{3/2}x}{\sqrt{\upsilon}}$ is Weissenberg number.

The wall share stress at the surface using boundary approximations is

$$\tau_w=\frac{1}{\sqrt{2}}\mu_0\Gamma\left(\frac{\partial u}{\partial y}\right)^2+\mu_0\frac{\partial u}{\partial y},\quad q_w=-k\frac{\partial T}{\partial y}+q_r,\quad \text{at } y=0. \tag{18}$$

Nusselt number and skin friction coefficients are defined as

$$Nu_x=\frac{xq_w}{k(T_w-T_\infty)},\quad C_f=\frac{\tau_w}{\rho U^2}. \tag{19}$$

In dimensionless form

$$\frac{Nu_x}{\sqrt{\mathrm{Re}_x}}=-[1+R]\Theta'(\xi)_{\xi=0},$$
$$\sqrt{\mathrm{Re}_x}C_f=[\frac{1}{\sqrt{2}}W_e^2(f''(\xi))^2+f''(\xi)]_{\xi=0},\quad \mathrm{Re}_x=x\sqrt{\frac{a}{\upsilon}}. \tag{20}$$

3. Numerical solution

The existing magnetized fluid flow over the microcantiliver sensor-based surfaces generates a highly intricated mathematical nonlinear

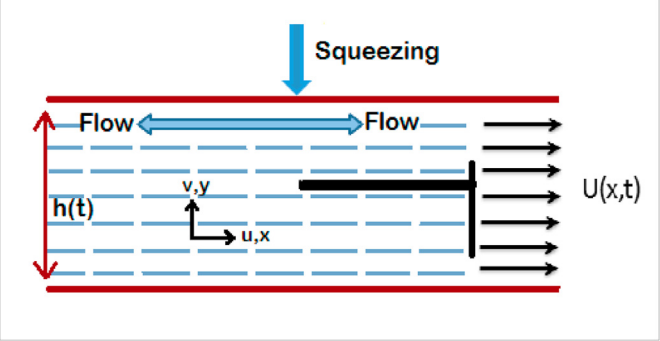

Figure 1. Physical representation of sensor surface.

system which then distorted into a simplified form by the assistance of similarity transformations. The nonlinear Eqs. (15) and (16) with transformed boundary conditions (17) are then treated numerically to acquire the solutions with the assistance of a well-known efficient RK-4 numerical method integrated with the Shooting approach. The descending order technique was followed by this numerical scheme i.e. by altering higher-order differential equations to first ordinary order differential equations. Moreover, the boundary of the flow channel was selected very carefully.

$$x_1 = f, \quad x_2 = f', \quad x_3 = f'', \quad x_4 = \Theta, \quad x_5 = \Theta'. \tag{21}$$

Therefore, the system becomes as

$$x_1' = x_2, \quad x_2' = x_3,$$

$$x_3' = \frac{1}{(1+\sqrt{2}nx_3W_e^2)}\Big[\frac{x_5}{x_4-\Theta_r}x_3 + \frac{1}{\sqrt{2}}W_e^2\frac{x_5}{x_4-\Theta_r}(x_3)(x_3)^2 - \frac{x_4-\Theta_r}{\Theta_r}((x_2)^2 \tag{22}$$

$$-\frac{b\xi}{2}x_3 - 1 + b(1-x_2) - x_1x_3 + M(x_2-1) - x_1x_3)\Big],$$

$$x_4' = x_5,$$

$$x_5' = \frac{-1}{(1+R+\epsilon x_4 - \frac{\beta b^2 \Pr \xi^2}{4} - \beta \Pr(x_1)^2 - \beta b \Pr \xi x_1)}\Big[\Pr\Big(x_1 + \frac{b\xi}{2} - \frac{\beta b^2 \xi}{4} \tag{23}$$

$$+3\beta x_1x_2 + \frac{\beta b\xi x_2}{2} - \frac{\beta b x_1}{2}\Big)x_5 + \Pr\Big(x_2 - \frac{b}{2} + \frac{\beta b^2}{4} - \beta(x_1)^2$$

$$+\frac{\beta b\xi x_3}{2} + \beta b x_2 - \beta b x_1 + \beta x_1x_3 + Q\Big)x_4\Big],$$

with initial conditions

$$x_1(0) = -f_0, \quad x_2(0) = 0, \quad x_5(0) = -1, \quad x_2(\xi) \to 1, \quad x_4(\xi) \to 0 \text{ when } \xi \to \infty. \tag{24}$$

To develop the solutions of this model total five initial conditions are necessary but only three are specified above. Two initial conditions are required to have $m_2(\xi) \to 1, m_4(\xi) \to 0$ when $\xi \to \infty$. So, it is accepted that $m_2(0) = s_1$, and $m_5(0) = s_2$ are two other conditions. Moreover, the

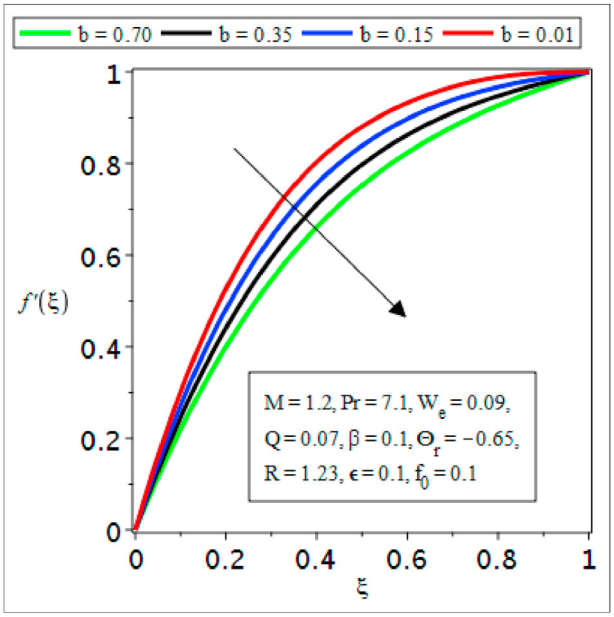

Figure 2. Behavior of *b* on velocity distribution.

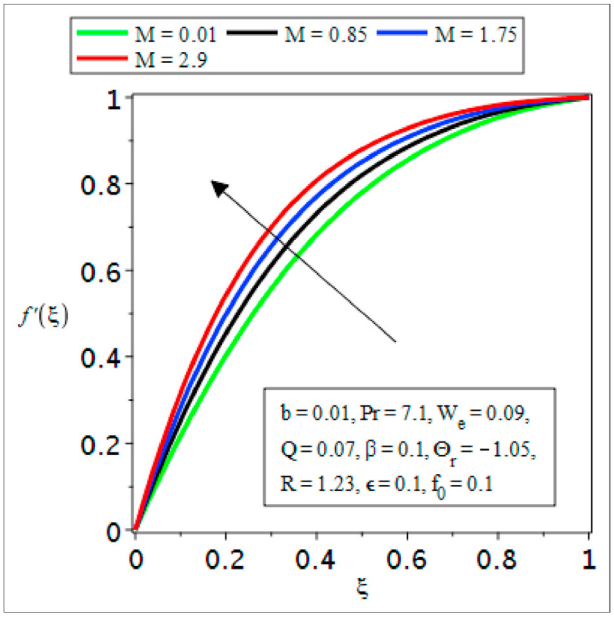

Figure 3. Effects of M on velocity distribution.

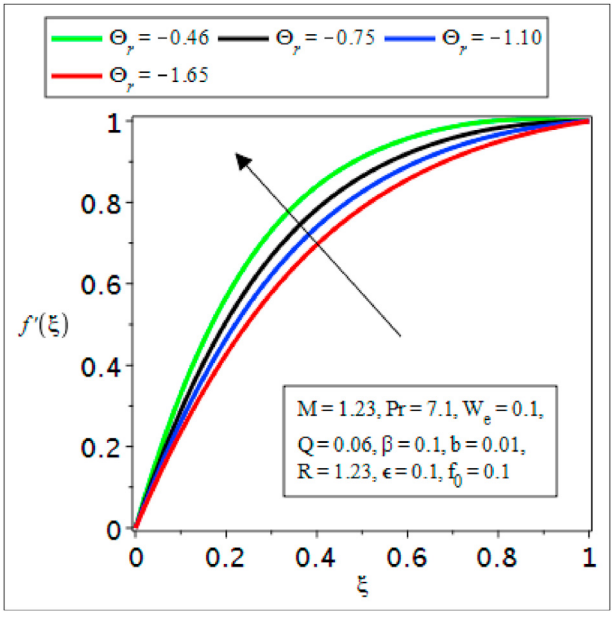

Figure 4. Impact of Θ_r on velocity profile.

Newton-Raphson scheme is effectually used to determine the suitable values of s_1 and s_2 by accounting the physical parameters and conditions related to boundary region. The convergence criteria and step length for current investigation are 10^{-5} and h = 0.01.

4. Results and discussions

The nonlinear system of differential type equations with suitable boundary conditions is computed with the assistance of the numerical technique namely shooting technique. The numerical consequences are attained for diverse values of the emergent controlled parameters, namely, heat generation parameter Q, power-law number n, Weissenberg index W_e, magnetic parameter M, thermal relaxation parameter β, the squeeze number b, radiation parameter R, and Prandtl number Pr. To scrutinize the convergence of these consequential parameters over the

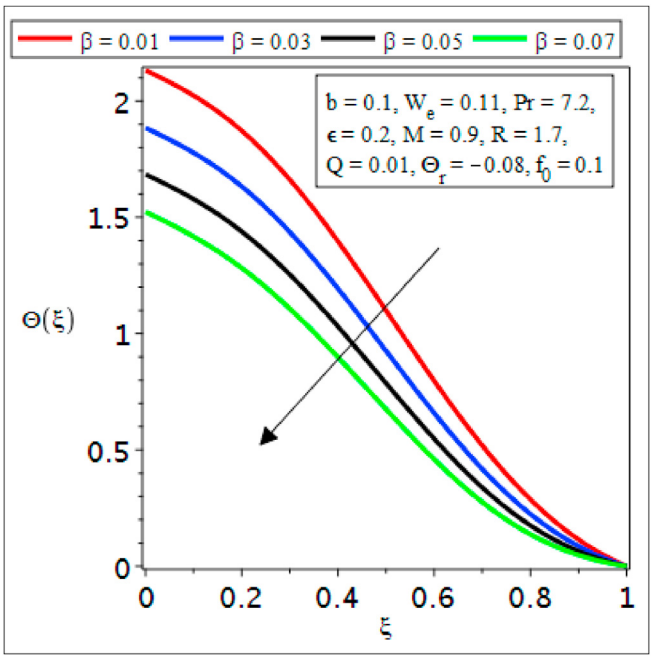

Figure 5. Sway of β on temperature distribution.

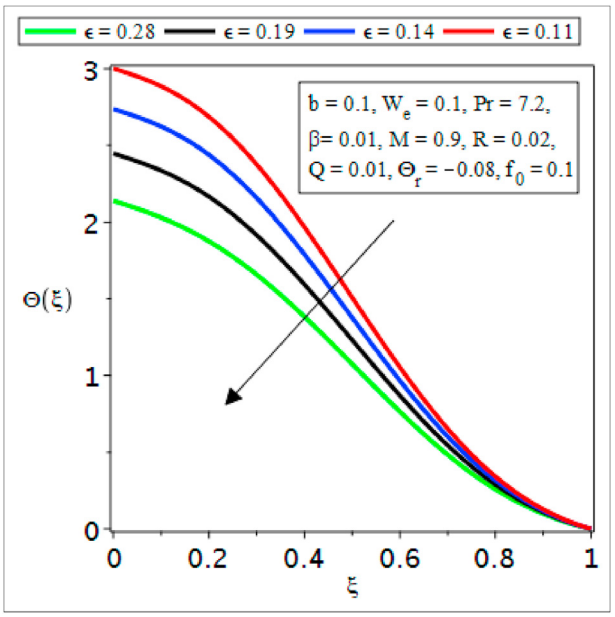

Figure 7. Conduct of temperature curve for ε

temperature and velocity profiles a comprehensive graphical discussion is presented. From Figure 1 the complete flow structure of the phenomenon can be visualized. The sensor-based surface is sited in a locally free stream. Figure 2 clearly depicts that the inverse relation of squashed flow number *b* and the squeezed power *a* causes the reduction in the particles's kinetic energy that results in the decreasing of the velocity profile. Moreover, the duel behaviour of velocity is observed due to various variations in the boundary region. As the magnetic effect M stimulates the particles in a single path that prorogates the motion of the particles as an outcome the velocity profile upsurges as revealed in Figure 3. Physically, an escalation in the magnetic parameter upsurges a resistance towards the axial flow channel, since in the present case the upper plate is in squashing condition, so, this physical situation eliminates the influence of exerted strength on the velocity filed which results in enhancing the fluid velocity through the channel. Moreover, the growing magnetic parameter produces a positive impact on the boundary layer. Figure 4 describes the direct association between Θ_r and velocity profile. For the mounting value of Θ_r, the velocity curve moves upward. The temperature declination can be analyzed for rising values of β in Figure 5. Physically, the parameter β represents the variance between the liquids and solids. The smaller values of parameter β shows the fluid nature while the larger values lead to viscoelastic solids. As β has direct relation to the squeezed strength so for increment in β retards the movement of fluid molecules which consequently decreases the fluid temperature. It is marvelous that same for velocity distribution the temperature diminishes for intensifying values of squashed flow number *b* as displayed in Figure 6. Physically, greater values *b* diminishes the squashed force on the fluid velocity which subsequently lessens the fluid temperature. So, it is obvious that the thermal boundary layer width varies inversely to squeezed flow index *b*. It is perspicuous from Figure 7 that the temperature curve moves

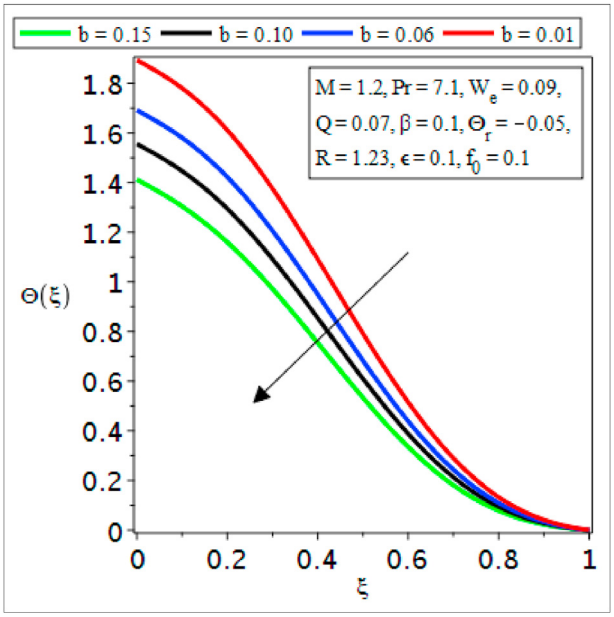

Figure 6. Effects of b on temperature field.

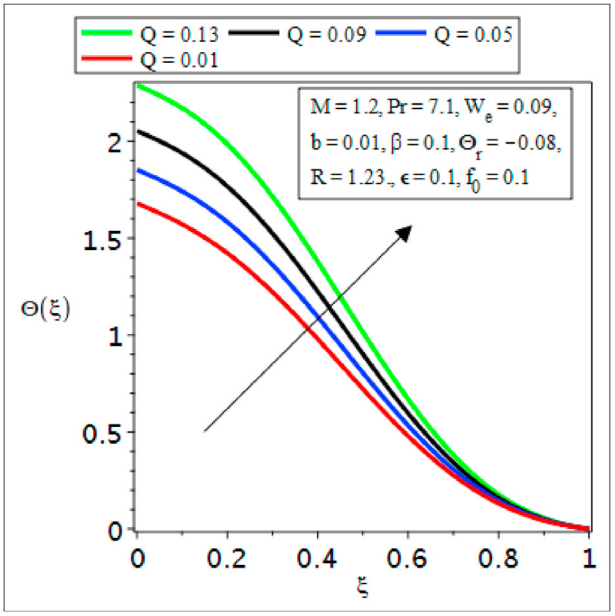

Figure 8. Impact of *Q* on temperature curve.

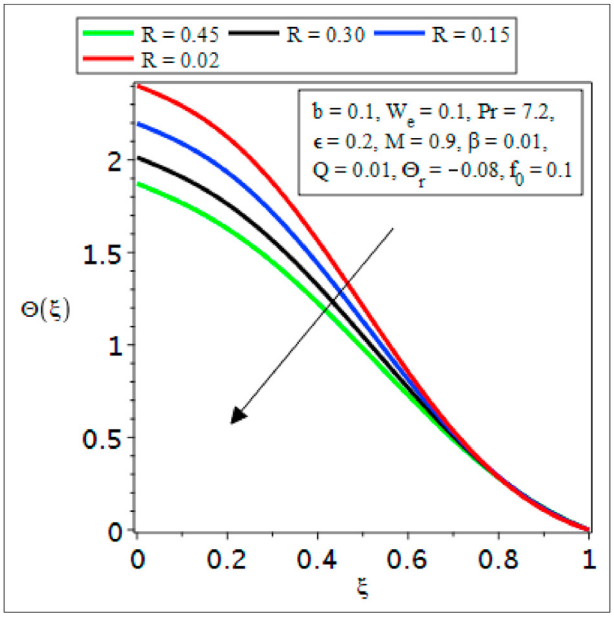

Figure 9. Variation of temperature for R.

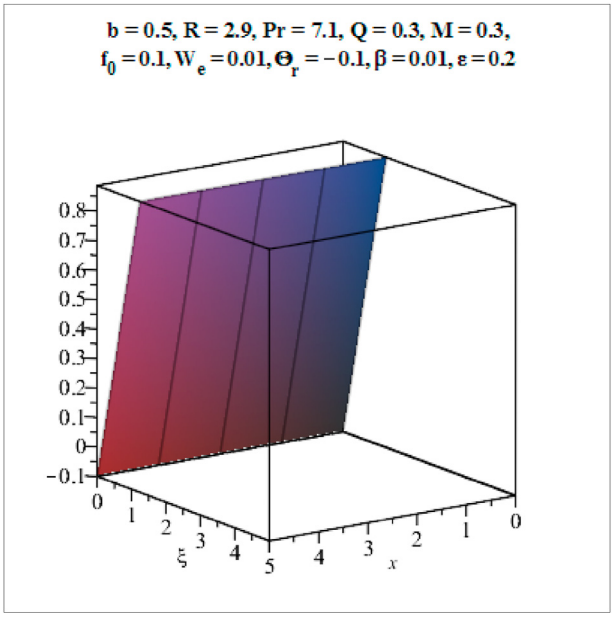

Figure 11. Three-dimensional graph when b = 0.5.

downward for accelerating values of ε. The reason for such behavior is the inverse relation of ε with temperature. Figure 8 delineates the conduct of heat generation on temperature distribution. The profile of temperature is descending for increasing values of Q. Figure 9 shows that reduction in fluid temperature occurs for enlarging values of R. This is due to the reason that the temperature transfer from the upper surface to the environment resulting a reduction in the fluid temperature. Figures 10, 11, and 12 clearly represent the 3-D structure for distinct values of parameter b. For a bigger value of parameter b sudden change in 3-D shape occurs. Figures 13, 14, and 15 delineate the streamlines for the ascending values of index b. It is flawless from the graphs that streamlines are moving away from the axis for rising values of b. Figure 16 clearly depicts the consequences of W_e, and b on the value of skin friction coefficient. The curve of coefficient of skin friction moves upward due to

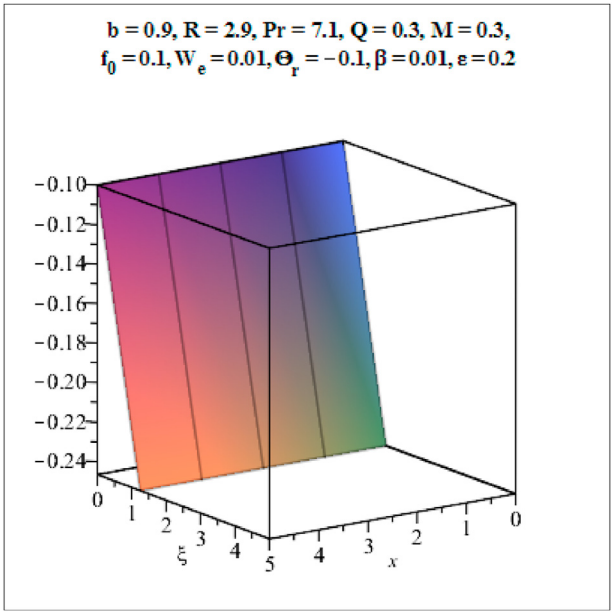

Figure 12. Three-dimensional graph when b = 0.9.

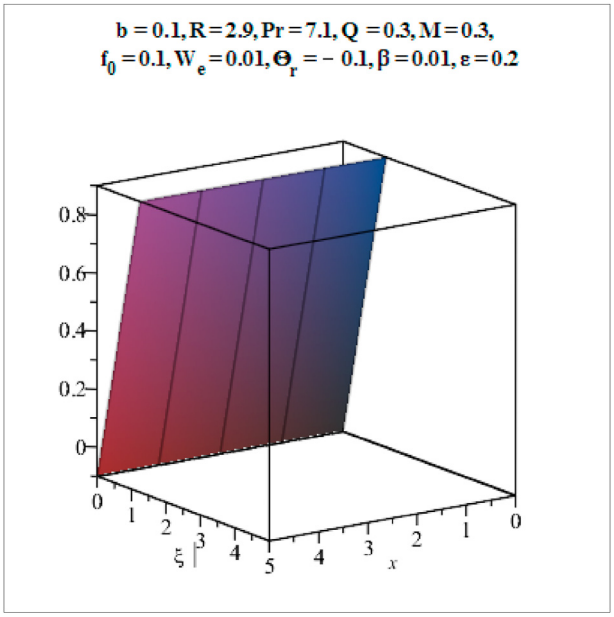

Figure 10. Three-dimensional graph when b = 0.1.

accretion in W_e. For the distinct values of flow index variable b, power number n and Weissenberg index W_e the corresponding skin friction results can be envisioned from Table 1. It is eminent that for enlarging values of b and presuming W_e and n persistent produces a reduction in the value of skin friction coefficient while its value growing for the variation of Weissenberg number W_e.

5. Validity of numerical code

The accuracy of the current numerical code is tested by validating the contemporary solutions with the solutions of T. Salahuddin and M.Y. Malik [37]. The validation of equations is found for various parameters such as squeezed flow index parameter b and magnetic parameter M. It is found from the comparison of figures that both temperature and velocity fields are moving downwards for increasing the value of parameter b.

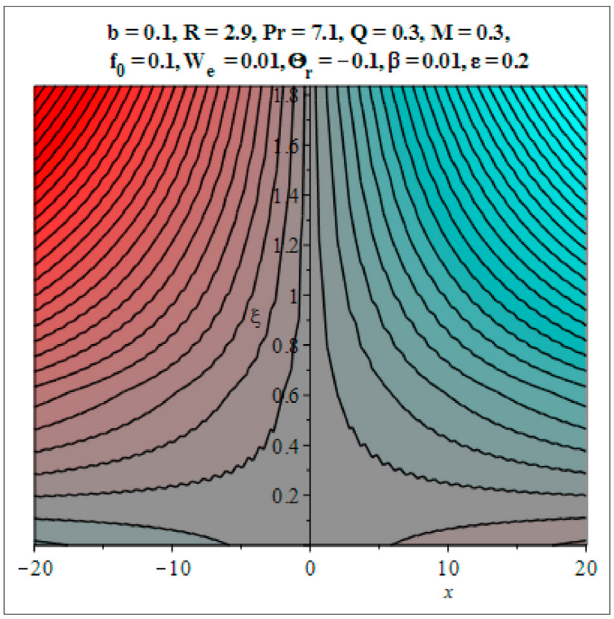

Figure 13. Streamlines for b = 0.1.

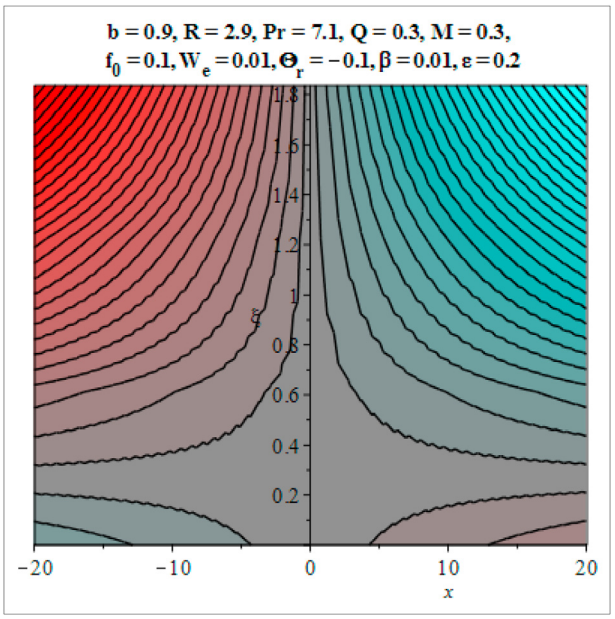

Figure 15. Streamlines for b = 0.9.

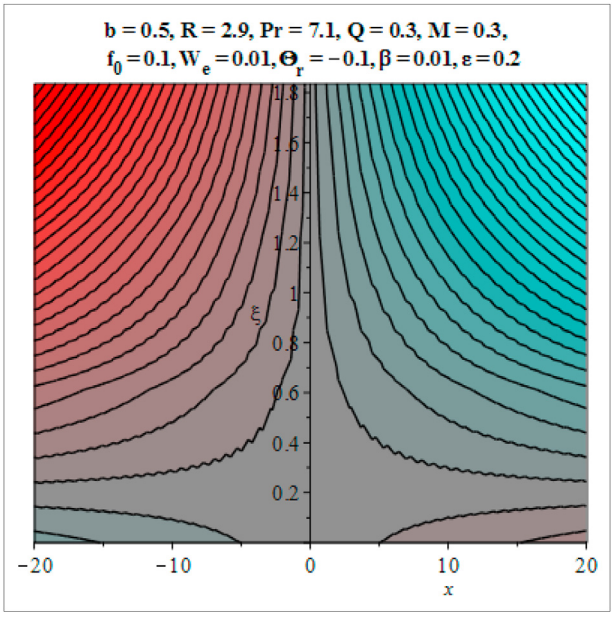

Figure 14. Streamlines for b = 0.5.

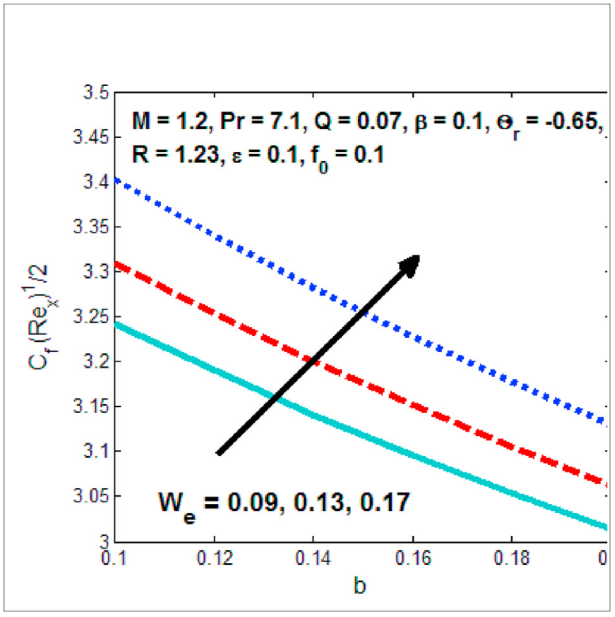

Figure 16. The impact of b and W_e on skin friction $C_f \mathrm{Re}_x^{1/2}$.

Table 1. Values of coefficient of skin friction relative to b and W_e.

b	W_e	$C_f \mathrm{Re}_x^{1/2}$
0.01	0.09	3.518321
0.02		3.483602
0.03		3.449919
0.01		3.518326
	0.13	3.610309
	0.17	3.739160

6. Concluding remarks

Due to the great importance of microcantilever sensor surfaces, we have presented a magneto hydro-dynamically squashed flow of Williamson fluid across a microcantilever sensor-based surface. Microcantilevers have gained significant potential applications in various sciences ranging from chemical and physical sensing to diagnosing biological diseases. The technology grasps the key to the coming generation of extremely sensitive sensors. The energy equation has constructed with the help of C-CHFM. The solutions to governing equations have been gained by using the numerical techniques. The following are the essential points:

1. The kinematics viscosity parameter Θ_r, magnetic parameter M are the factors that cause an increment in the velocity profile while the squeezed flow index b lessens the velocity profile.
2. The temperature curve moves downward for growing values of b, R and ε but it can be seen from figs. that temperature curve moves upward for rising values of Q and β.
3. For the distinct values of flow index variable b, power-law number n, and Weissenberg index W_e the corresponding skin friction results can be envisioned from Table 1. It is eminent that for intensifying values of b and presuming W_e and n persistent produces a reduction in the value of skin friction coefficient, while skin friction values are emerging for the variation of Weissenberg number W_e.
4. Moreover, the accuracy of the sensor is enhanced by hydromagnetic and wall penetrable velocity effects until the chemical impeding at sensor-based surface is not repressed by upsurges in flow related to these properties.

Declarations

Author contribution statement

Azad Hussain: Conceived and designed the analysis.
Rabia Zetoon: Analyzed and interpreted the data.
Shoaib Ali: Analyzed and interpreted the data; Wrote the paper.
S. Nadeem: Contributed analysis tools or data.

Funding statement

This research did not receive any specific grant from funding agencies in the public, commercial, or not-for-profit sectors.

Competing interest statement

The authors declare no conflict of interest.

Additional information

No additional information is available for this paper.

References

[1] Muhammad Usman, Muhammad Hamid, Rizwan Ul Haq, Wei Wang, Heat and fluid flow of water and ethylene-glycol based Cu-nanoparticles between two parallel squeezing porous disks: LSGM approach, Int. J. Heat Mass Tran. 123 (2018) 888–895.
[2] M. Atlas, Rizwan Ul Haq, T. Mekkaoui, Active and zero flux of nanoparticles between a squeezing channel with thermal radiation effects, J. Mol. Liq. 223 (2016) 289–298.
[3] Mair Khan, M.Y. Malik, T. Salahuddin, Arif. Hussian. Heat and mass transfer of Williamson nanofluid flow yield by an inclined Lorentz force over a nonlinear stretching sheet, Results Phys. 8 (2018) 862–868.
[4] M. Sheikholeslami, M.M. Rashidi, Dhafer M. Al Saad, F. Firouzi, Houman B. Rokni, G. Domairry, Steady nanofluid flow between parallel plates considering thermophoresis and Brownian effects, J. King Saud Univ. Sci. 28 (2016) 380–389.
[5] Rizwan Ul Haq, S. Nadeem, Z.H. Khan, N.F.M. Noor, MHD squeezed fow of water functionalized metallic nanoparticles over a sensor surface, Phys. E Low-dimens. Syst. Nanostruct. 73 (2015) 45–53.
[6] K. Ganesh Kumar, B.J. Gireesha, M.R. Krishanamurth, N.G. Rudraswamy, An unsteady squeezed flow of a tangent hyperbolic fluid over a sensor surface in the presence of variable thermal conductivity, Results Phys. 7 (2017) 3031–3036.
[7] Mair Khan, M.Y. Malik, T. Salahuddin, Imad Khan, Heat transfer squeezed flow of Carreau fluid over a sensor surface with variable thermal conductivity: a numerical study, Results Phys. 6 (2016) 940–945.
[8] M.M. Rashidi, H. Shahmohamadi, S. Dinarvand, Analytic approximate solutions for unsteady two-dimensional and axisymmetric squeezing flows between parallel plates, Math. Probl Eng. (2008) 935095.
[9] Imad Khan, Shafquat Ullah, M.Y. Malik, Arif Hussain, Numerical analysis of MHD Carreau fluid flow over a stretching cylinder with homogenous-heterogeneous reactions, Results Phys. 9 (2018) 1141–1147.
[10] S. Bilal, Khalil-ur-Rehman, M.Y. Malik, Arif Hussain, Mair Khan, Effects of temperature dependent conductivity and absorptive/generative heat transfer on MHD three dimensional flow of Williamson fluid due to bidirectional non-linear stretching surface, Results Phys. 7 (2017) 204–212.
[11] M.Y. Malik, A. Hussain, T. Salahuddin, M. Awais, S. Bilal, F. Khan, Flow of Sisko fluid over a stretching cylinder and heat transfer with viscous dissipation and variable thermal conductivity: a numerical study, AIP Adv. 6 (2016), 045118.
[12] M.Y. Malik, M. Bibi, F. Khan, T. Salahuddin, Numerical solution of Williamson fluid flow past a stretching cylinder and heat transfer with variable thermal conductivity and heat generation/absorption, AIP Adv. 6 (2016), 035101.
[13] Khalil Ur Rehman, M.Y. Malik, T. Salahuddin, M. Naseer, Dual stratified mixed convection flow of Eyring-Powell fluid over an inclined stretching cylinder with heat generation/absorption effect, AIP Adv. 6 (2016), 075112.
[14] M.Y. Malik, A. Hussain, T. Salahuddin, M. Awais, S. Bilal, Numerical solution of Sisko fluid over a stretching cylinder and heat transfer with variable thermal conductivity, J. Mech. 32 (2016) 593–601.
[15] M.Y. Malik, T. Salahuddin, A. Hussain, S. Bilal, M. Awais, Homogeneous-heterogeneous reactions in Williamson fluid MHD squeezed flow of Carreau-Yasuda fluid model over a stretching cylinder by using Keller box method 10 (2015) 107227.
[16] A.R.A. Khaled, K. Vafai, Hydromagnetic squeezed flow and heat transfer over a sensor surface, Int. J. Eng. Sci. 42 (2004) 509–519.
[17] T. Salahuddin, M.Y. Malik, A. Hussain, S. Bilal, M. Awais, Effects of transverse magnetic field with variable thermal conductivity on tangent hyperbolic fluid with exponentially varying viscosity, AIP Adv. 5 (2015) 127103.
[18] C. Cattaneo, Sulla Conduzione del calore, Atti Semin Mat Fis Univ Modea Reggio Emilia 3 (1948) 83–101.
[19] C.I. Christov, On frame indifferent formulation of the Maxwell-Cattaneo model of finite speed heat conduction, Mech. Res. Commun. 36 (2009) 481–486.
[20] M.Y. Malik, M. Khan, T. Salahuddin, I. Khan, Variable viscosity and MHD flow in Casson fluid with Cattaneo-Christov heat flux model: using Keller box method, Eng. Sci. Technol. Int. J. 19 (2016) 1985–1992.
[21] T. Salahuddin, M.Y. Malik, A. Hussain, S. Bilal, M. Awais, MHD flow of Cattaneo-Christov heat flux model for Williamson fluid over a stretching sheet with variable thickness: using numerical approach, J. Magn. Magn Mater. 401 (2016) 991–997.
[22] T. Hayat, Ijaz Khan, A. Alsaedi, M. Waqas, Tabassam Yasmeen, Impact of Cattaneo–Christov heat flux model in flow of variable thermal conductivity fluid over a variable thicked surface, Int. J. Heat Mass Tran. 99 (2016) 702–710.
[23] T. Hayat, Ijaz Khan, A. Alsaedi, M. Farooq, Tabassam Yasmeen, Stagnation point flow with Cattaneo-Christov heat flux and homogeneous-heterogeneous reactions, J. Mol. Liq. 220 (2016) 49–55.
[24] Muhammad Ijaz Khan, Muhammad Waqas, Tasawar Hayat, Ahmed Alsaedi, A comparative study of Casson fluid with homogeneous-heterogeneous reactions, J. Colloid Interface Sci. 498 (2017) 85–90.
[25] T. Hayat, Ijaz Khan, Sumaira Qayyum, Ahmed Alsaedi, Entropy generation in flow with silver and copper nanoparticles, Colloid. Surface. Physicochem. Eng. Aspect. 539 (2018) 335–346.
[26] T. Hayat, Ijaz Khan, Sumaira Qayyum, Ahmed Alsaedi, Entropy generation in magnetohydrodynamic radiative flow due to rotating disk in presence of viscous dissipation and Joule heating, Phys. Fluid. 30 (2018), 17101.
[27] M. Waleed Ahmed Khan, T. Hayat, Ijaz Khan, Alsaedi Ahmed, Entropy generation minimization (EGM) of nanofluid flow by a thin moving needle with nonlinear thermal radiation, Phys. B Condens. Matter 534 (2018) 113–119.
[28] Niaz B. Khan, Zainah Ibrahim, M. Ijaz Khan, T. Hayat, Muhammad F. Javed, VIV study of an elastically mounted cylinder having low mass-damping ratio using RANS model, Int. J. Heat Mass Tran. 121 (2018) 309–314.
[29] T. Hayat, Ijaz Khan, Sumaira Qayyum, Alsaedi Ahmed, Modern developments about statistical declaration and probable error for skin friction and Nusselt number with copper and silver nanoparticles, Chin. J. Phys. 55 (2017) 2501–2513.
[30] T. Hayat, Mumtaz Khan, Muhammad Ijaz Khan, Alsaedi Ahmed, Muhammad Ayub, Electromagneto squeezing rotational flow of Carbon (Cu)-Water (H2O) kerosene oil nanofluid past a Riga plate: a numerical study, PloS One (2017).
[31] Zahir Shah, Ebraheem O. Alzahrani, Abdullah Dawar, Asad Ullah, Ikramullah Khan, Influence of Cattaneo-Christov model on Darcy-Forchheimer flow of Micropolar Ferrofluid over a stretching/shrinking sheet, Int. Commun. Heat Mass Tran. 110 (2020) 104385.
[32] Muhammad Wakeel Ahmad, Poom Kumam, Zahir Shah, Ali Ahmad Farooq, Rashid Nawaz, Abdullah Dawar, Saeed Islam, Phatiphat Thounthong, Darcy–Forchheimer MHD couple stress 3D nanofluid over an exponentially stretching sheet through cattaneo–christov convective heat flux with zero nanoparticles mass flux conditions, Entropy 21 (2019) 867.
[33] Zahir Shah, Abdullah Dawar, Ebraheem Alzahrani, Saeed Islam, Hall effect on couple stress 3D nanofluid flow over an exponentially stretched surface with cattaneo Christov heat flux model, IEEE 7 (2019) 64844–64855.
[34] Zahir Shah, Abdullah Dawar, I. Khan, Saeed Islam, Dennis Ling, Chaun Ching, Aurang Zeb Khan, Cattaneo-Christov model for electrical magnetite micropoler Casson ferrofluid over a stretching/shrinking sheet using effective thermal conductivity model, Case Stud. Therm. Eng. 13 (2019) 100352.
[35] D. Knezevic, V. Svic, Mathematical modelling of changing of dynamical viscosity, as a function of temperature and pressure, of mineral oils for hydralic systems, Facta. Univ. 6 (2006) 27–34.
[36] F.C. Lai, F.A. Kulacki, The effect of variable viscosity on convective heat transfer along a vertical surface in a saturated porous medium, Int. J. Heat Mass Tran. 33 (1990) 1028–1031.
[37] T. Salahuddin, Arif Hussain, S. Bilal, M. Awais, Imad Khan, M.Y. Malik, MHD squeezed flow of Carreau-Yasuda fluid over a sensor surface, Alexandria Eng. J. 56 (2017) 27–34.